communications biology

Article

https://doi.org/10.1038/s42003-024-07007-6

Neural, genetic, and cognitive signatures of creativity

Check for updates

Cheng Liu[1], Kaixiang Zhuang[2], Daniel C. Zeitlen[3], Qunlin Chen[1], Xueyang Wang[1], Qiuyang Feng[1], Roger E. Beaty[3] & Jiang Qiu[1]

Creativity is typically operationalized as divergent thinking (DT) ability, a form of higher-order cognition which relies on memory, attention, and other component processes. Despite recent advances, creativity neuroscience lacks a unified framework to model its complexity across neural, genetic, and cognitive scales. Using task-based fMRI from two independent samples and MVPA, we identified a neural pattern that predicts DT, validated through cognitive decoding, genetic data, and large-scale resting-state fMRI. Our findings reveal that DT neural patterns span brain regions associated with diverse cognitive functions, with positive weights in the default mode and frontoparietal control networks and negative weights in the visual network. The high correlation with the primary gradient of functional connectivity suggests that DT involves extensive integration from concrete sensory information to abstract, higher-level cognition, distinguishing it from other advanced cognitive functions. Moreover, neurobiological analyses show that the DT pattern is positively correlated with dopamine-related neurotransmitters and genes influencing neurotransmitter release, advancing the neurobiological understanding of creativity.

Creativity aids in the development of individual problem-solving skills and is critical to the cultural and economic advancement of society. Divergent thinking (DT), the ability to produce multiple ideas on an open-ended task, plays an essential role in creativity; indeed, creative ability is typically operationalized by performance on DT tasks[1]. DT may also help people to develop an understanding of differences and an appreciation of different perspectives[2], have a positive impact on mood[3], and can serve as an indicator of representative potential[4–7].

There are both consistent and inconsistent conclusions in task-related functional magnetic resonance imaging (fMRI) studies of DT. The most active brain regions are centered on the bilateral dorsolateral prefrontal cortex (DLPFC), the ventrolateral prefrontal cortex (VLPFC) and right anterior cingulate cortex (ACC)[8–13]. However, significant activation of other brain regions has also been found in different studies, such as the right angular gyrus (AG)[10], the left fusiform gyrus (FG)[8,10] and the left middle temporal gyrus (MTG)[9,13,14]. This variability may be attributed to the fact that creativity represents the highest level of advanced cognition, requiring the coordination of multiple cognitive processes and the involvement of corresponding brain regions during creative thinking. Benedek et al. [15–18], Functional connectivity, in conjunction with the dual-process theory of creativity, explains DT at the network level. The dual-process theory of creativity posits that creative thinking involves both spontaneous and unconscious processes of idea generation and connection supported by the default model network (DMN), such as mind-wandering and free association[19,20], as well as the conscious evaluation and selection of generated answers supported by the frontoparietal control network (FPCN)[15,21]. The close collaboration between the DMN and FPCN networks facilitates the emergence of creative thought and constitutes a core mechanism of this complex cognitive process[21–23]. However, in addition to discretely dividing brain regions based on function, morphology, and other attributes[24], a contemporary direction in neuroimaging research suggests that the mature adult cerebral cortex is organized as a series of smoothly varying continuous gradients. Notably, the primary gradient represents an organizational framework that transitions from sensory processing to abstract cognition[25]. As a complex cognitive process involving multiple brain regions, the neural representation of creative thinking is well-suited to be explained using a continuous gradient approach, which we refer to in this study as the organizing principle of neural representation.

Cognitive decoding offers a powerful approach for elucidating the complexity of DT. By leveraging quantitative reverse inference, cognitive decoding maps activation patterns in neuroimaging data onto psychological concepts that characterize the higher-level mental processes engaged[26]. In addition, human cognition is strongly influenced by genetics and neurotransmitters[27–29]. Integrating this understanding with neuroimaging

[1]Key Laboratory of Cognition and Personality of Ministry of Education, Faculty of Psychology, Southwest University, Chongqing, China. [2]Institute of Science and Technology for Brain-Inspired Intelligence, Fudan University, Shanghai, China. [3]Department of Psychology, Pennsylvania State University, Pennsylvania, USA. e-mail: qiuj318@swu.edu.cn

techniques can provide deeper insights into the neurobiological mechanisms that underlie complex behavioral traits[30]. However, systematic applications of these approaches to creativity research are still limited, as few studies have attempted to integrate neuroimaging and genetic approaches[31].

In the present study, we used MVPA-based neural decoding techniques to construct the neural representation of DT in two samples (sample 1 [$n = 55$] and sample 2 [$n = 30$]) and attempt to decipher the principles of its neural organizations. MVPA allows for capturing information at a more refined spatial scale[32] and has been shown to yield larger effect sizes in brain-outcome associations compared to univariate analysis[33]. Next, we explained the neural representations of DT from a cognitive decoding as well as a biogenetic perspective, by examining spatial correlations between the DT neural pattern and previously collected, open-source brain data on cognition, gene expression profiles, and neurotransmitter receptors and transporters. Finally, to extend the analyses from the group-level, we predicted individual DT scores from the DT brain pattern in the two task-based samples, and also from functional connectivity between the regions of the DT pattern across three large resting-state fMRI samples (SLIM = 410, GBB = 304, BBP = 600) (Fig. 1b). This systematic evaluation collectively contributes to our understanding of the neurobiological foundations of creativity.

Results

Decoding the neural basis of divergent thinking

To identify the multivariate patterns of fMRI activation for DT, we applied linear support vector machines (SVMs) to discriminate the novel use (NU) condition (i.e., DT) versus the general use (GU) control condition with a 10 × 10-fold cross-validation in the sample1 ($n = 55$) and sample2 ($n = 30$) respectively (see 'Methods' for details). In the classification of model1, the accuracy was 80% ± 3.8% (mean ± SE, $p < 0.00001$) and area under the receiver operating characteristic curve (AUC) was 0.90 with a sensitivity of 80.0% (95% CI: 70%–90%) and specificity of 80.0% (95% CI: 69%–89%) in the test participants (Fig. 2a, b). In the classification of model2, the accuracy was 85% ± 4.6% (mean ± SE, $p < 0.00001$) and the AUC was 0.94 with a sensitivity of 96% (95% CI: 89%–100%) and specificity of 73% (95% CI: 56%–89%) in the test participants (Fig. 2d, e).

To test whether a classification score was significant, we performed a permutation analysis: we first randomly reassigned subject labels and then performed tenfold cross-validation classification. Then, two samples were used to as validation dataset for each other to further test the generalization performance of two models, with no further model fitting (see 'Methods' for details). The results showed the accuracy of model1 when used sample2 as the validation dataset was 70% ± 5.9% (mean ± SE, $p = 0.0027$) (Fig. 2c). The accuracy of model2 when used sample1 as the validation dataset was 78% ± 3.9% (mean ± SE, $p < 0.00001$) (Fig. 2f). Altogether, the machine learning models achieved good accuracy across both samples, indicating reliable prediction of the DT (novel use) condition from multivariate patterns of fMRI activation.

To identify significant features that reliably contribute to the classification of NU and GU in model1 and model2, we conducted bootstrap tests with 10,000 iterations respectively (see 'Methods' for details). Then we obtain the thresholded maps of the two models. To statistically compare the two thresholded maps, we calculated Pearson correlation across voxel weights. The two pattern classifiers were high correlated with each other (Fig. 3a, $r = 0.838$, $p < 0.001$). Thus, we averaged the thresholded weight maps of the two models as the DT brain pattern (Fig. 3b, thresholded at $q < 0.05$ with a false discovery rate [FDR] correction). We found that NU versus GU was predicted by increased activity in bilateral DLPFC, bilateral dorsomedial prefrontal cortex (DMPFC), left VLPFC, bilateral ACC, bilateral orbitofrontal cortex (OFC), left AG, left MTG, bilateral thalamus, and right cerebellum (warm colors in Fig. 3b), and was predicted by decreased activity in right Superior Parietal Lobule, right Precuneus, and right inferior Lateral Occipital Cortex (cool colors in Fig. 3b).

To parse the cognitive processes involved in the DT brain pattern from a cognitive decoding perspective, we examined the spatial correlation between this pattern and meta-analytic fMRI activation maps (NeuroSynth datasets, see 'Methods'). For positive weights, the decoding results focus on Emotion, Cognitive, Memories, Judgments, Retrieval, and Reasoning; the results for negative weights focus on Visual, Selective, Location, Perception and Sensory (Fig. 3c) (see Supplementary Table 1). Thus, the DT brain

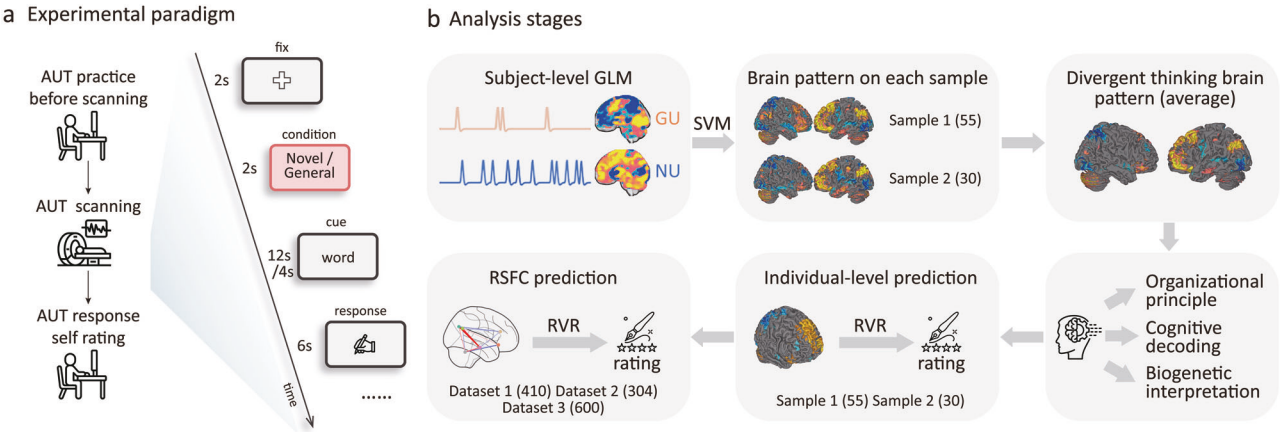

Fig. 1 | Experimental paradigms and analysis stages. a Sample 1 and sample 2 underwent two similar paradigms during fMRI acquisition. The task-based fMRI contained two conditions, the control condition and the DT condition, requiring subjects to generate a common or original use, respectively, for a given object. This procedure consisted of 4 runs (6 runs in sample 2), each run included 20 trials, comprised of 12 novel use prompts and 8 general use prompts. After the fMRI scan, subjects were asked to recall and refine their responses, and then rate the originality of their responses. **b** The analytic stages and datasets used in the present study. Specifically, a whole-brain multivariate pattern predictive of novel use vs general use was trained on the sample 1 ($N = 55$) and sample 2 ($N = 30$) using support vector machine and further evaluated in the two samples (via cross-validation and mutual use as a validation sample for each other). After identifying the DT brain activity pattern, we parsed the cognitive processes related to the brain pattern using meta-analytic decoding on Neurosynth. Then, we explored the neural organizational principle of the DT brain pattern by examining which brain networks the DT regions belonged to, as well as the spatial correlation with functional connectivity gradient maps. Next, to interpret the brain pattern from a biogenetic perspective, we explored spatial correlations between the DT brain pattern and gene expression as well as neurotransmitters. Finally, to extend from group-level findings to individual-level predictions, we used the DT brain pattern to predict individual DT scores in the two task-based fMRI samples and generalized the identified effects to resting-state modalities (across three large resting-state fMRI samples [dataset 1, $N = 410$; dataset 2, $N = 304$; dataset 3, $N = 600$]). Figure 1 was created entirely by the authors for this publication, without the use of any pre-existing elements or content from external sources.

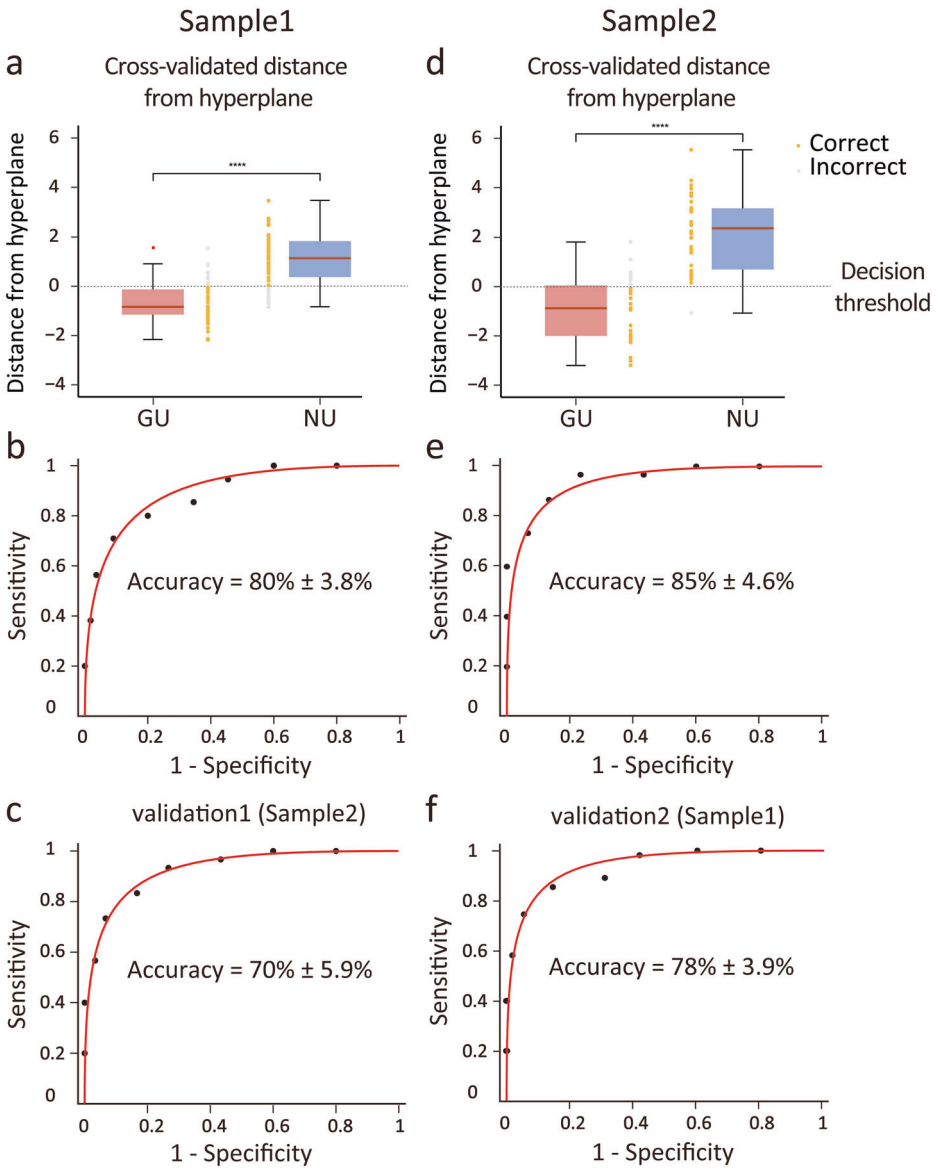

Fig. 2 | Predictive performance of the SVM models. a The cross-validated distance from hyperplane and the decision threshold of model1, the yellow dots indicate correct classification, and the gray dots indicate misclassification. **b** The receiver operating characteristic (ROC) plot of model1. The accuracy of the model1 was 80% ± 3.8%. **c** The ROC plot of model1 when sample2 as validation dataset. The accuracy of the model1 was 70% ± 5.9%. **d** The cross-validated distance from hyperplane and the decision threshold of model2. **e** The ROC plot of model2. The accuracy of the model2 was 85% ± 4.6%. **f** The ROC plot of model2 when sample1 as validation dataset. The accuracy of the model2 was 70% ± 5.9%. Source data are provided as a Supplementary Data file.

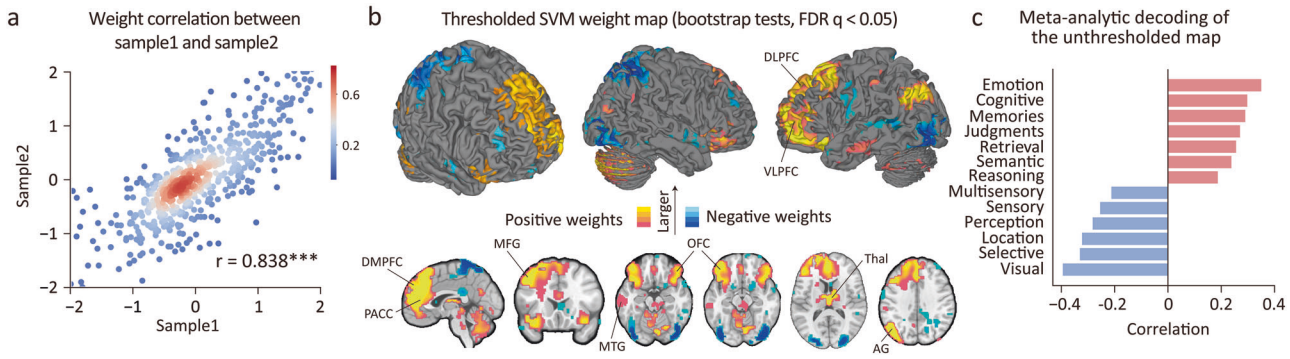

Fig. 3 | Divergent thinking brain pattern and cognitive decoding. a Pearson correlation between thresholded weights of two models. **b** The weight map shows the final predictive features after average the thresholded maps (significant feature weights of SVM models by the bootstrap tests and thresholded at an FDR of $q < 0.05$) of two models. **c** Decoding analysis based on a meta-analytic database. The bar plot shows the functional terms obtained from the Neurosynth decoder applied to the thresholded map. The pink bars represent the decoding results for positive weights, and the blue bars represent the decoding results for negative weights. The significance level is FDR-corrected $p < 0.05$. Source data are provided as a Supplementary Data file.

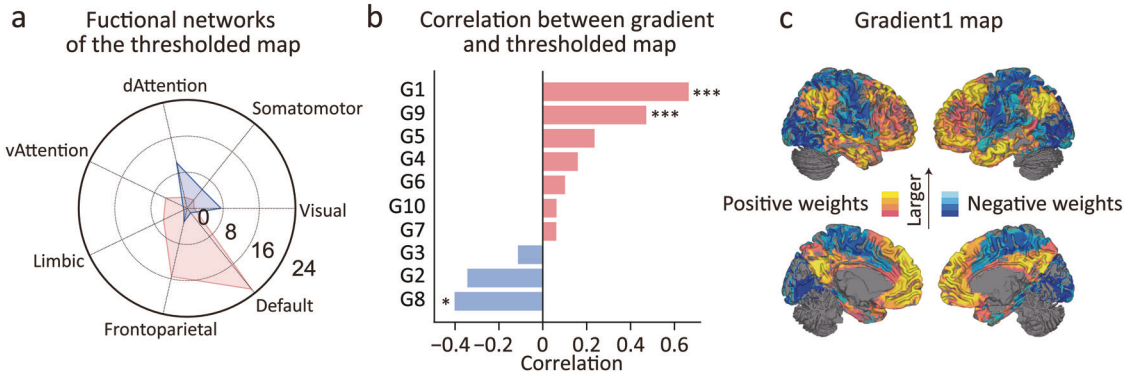

Fig. 4 | Neural organizational principle of DT brain pattern. a Overlap with large-scale resting-state functional networks. The radar chart depicts the posterior probability of observing overlaps between the thresholded SVM model and the resting-state functional networks. The pink chart represents the overlaps with the positive predictive weights of the model, and the blue chart represents the overlaps with the negative predictive weights of the model. **b** Correlation between gradient and the thresholded map. **c** Principle gradient map of functional connectivity. *** indicates FDR-corrected $p < 0.001$, * indicates FDR-corrected $p < 0.05$. Source data are provided as a Supplementary Data file.

pattern was positively associated with the neural bases of higher-order cognitive functions (e.g., memory and reasoning).

Mapping the neural signature of divergent thinking to functional gradients

In order to better integrate the results of the neural representations, we interpreted the distribution of brain regions for the DT brain pattern at the network level. Specifically, we examined which resting-state functional networks play important roles in the SVM model by calculating the proportions of overlap between the DT brain pattern (predictive weights) and each of the brain networks (see 'Methods' for details). The overlaps with the positive predictive weights of the model were focused on Default Model, Frontoparietal Control, and Limbic networks (Fig. 4a). The overlaps with the negative predictive weights of the model were focused on dorsal Attention, Visual and Somatomotor networks. These overlap results with functional brain networks suggest that the positive brain activity pattern for DT (i.e., the regions more involved in creative thinking) is concentrated in the default and frontal-parietal control networks.

Next, we tested if these brain activity patterns for DT map to an underlying organizing principle. Given the importance of gradients in understanding organizing principles of the brain, we examined the spatial correlation between the DT brain pattern and the first 10 gradients in the brain (see 'Methods' for details). We found significant positive correlations between the DT brain pattern and the principal gradient map ($r = 0.66$, $p_{fdr} = 0.0005$), the 9th gradient map ($r = 0.47$, $p_{fdr} = 0.0005$), and a significant negative correlation with the 8th gradient map ($r = -0.40$, $p_{fdr} = 0.0007$) (Fig. 4b, thresholded at $q < 0.05$ with FDR correction; for the full list, see Supplementary table 2). Thus, by mapping the neural signature of DT onto macroscale gradients, we situate creativity within the brain's primary system supporting complex psychological processes.

Linking the neural signature of divergent thinking to gene expression and neurotransmission

We next explored potential gene expression profiles (from Allen Human Brain Atlas datasets) that are associated with the DT brain pattern. First, we preprocessed the micro-array data according to a recommended pipeline[34] and obtained group-level gene expression maps that were normalized across samples and donors (15,633 genes). Second, we matched the gene expression maps to the DT brain pattern covering 574 regions (Fig. 5a). Then, we conducted a Pearson's correlation analysis to estimate the relationship between the DT brain pattern and each gene expression map (Fig. 5b). The significance of these correlations was obtained by permutation tests (10,000 times) in which spatial autocorrelations were preserved in the surrogate maps[35]. Finally, we performed Gene Ontology enrichment analysis for assessing the overrepresentation of gene sets in biological experiments to derive meaningful insights. The significance of the GO enrichment terms was further tested using a null model, which was generated by performing an enrichment analysis using surrogate maps which preserved the empirically observed spatial autocorrelations [35].

We found that genes within the gene set that showed significant enrichment were those involved in the negative regulation of multicellular organismal process, detoxification of copper ion and detoxification of inorganic compound (FDR-corrected, all $q < 0.05$, Fig. 5c; for the full list, see Supplementary Table 3). We also performed Gene Ontology enrichment analysis on a gene set made up of the genes ranked in reverse order (i.e., starting with the most significant negative correlation and ending with the most significant positive correlation), but did not find significant enrichment of any genes in this set. Taken together, these results indicate that the DT brain pattern is associated with the expression levels of genes that affect the overall functioning of the organism by influencing the synthesis and release of neurotransmitters and the transmission of information.

Furthermore, we assessed potential neurotransmitter receptors and transporters that are associated with the DT brain pattern. In this analysis, we calculated the spatial Pearson's correlation between the DT brain pattern and each receptors/transporters map (Fig. 5d), which were collected in previous studies via PET (see "Methods" for details). The significance of these correlations was obtained by permutation tests (10,000 times) in which spatial autocorrelations were preserved in the surrogate maps. We found that the neurotransmitter receptors/transporters that showed the most significant positive correlations were MOR ($r = 0.67$, $p_{spin} < 0.001$), CB_1 (omar) ($r = 0.45$, $p_{spin} < 0.001$), H_3 ($r = 0.41$, $p_{spin} < 0.001$), $mGluR_5$ ($r = 0.39$, $p_{spin} < 0.001$) (for the full list, see Supplementary Table 4). Thus, the DT brain pattern is related to neurotransmitters capable of promoting dopamine release.

Using the neural signature of DT to predict individual creativity during task performance

To validate the effectiveness of the brain pattern as biomarker for predicting DT we applied relevance vector regression (RVR) with single-trial beta maps (only NU condition for each subject) as feature to predict originality ratings for DT responses with a 10×10-fold cross-validation in the sample1 ($n = 55$) and sample2 ($n = 30$) (see 'Methods' for details). The prediction results of sample 1 are shown in Fig. 6a; the distribution of the correlation(r) between the predicted value and the true value in 10×10-fold cross-validations ranged from 0.21 to 0.39 (average $r = 0.35$, $p_{pt} < 0.001$, mean absolute error = 0.82). Figure 6b shows the prediction results of sample 2; the distribution of the correlation(r) between the predicted value and the true value in 10×10-fold cross-validations ranged from 0.09 to 0.17 (average $r = 0.14$, $p_{pt} < 0.001$, mean absolute error = 1.82). Thus, the DT

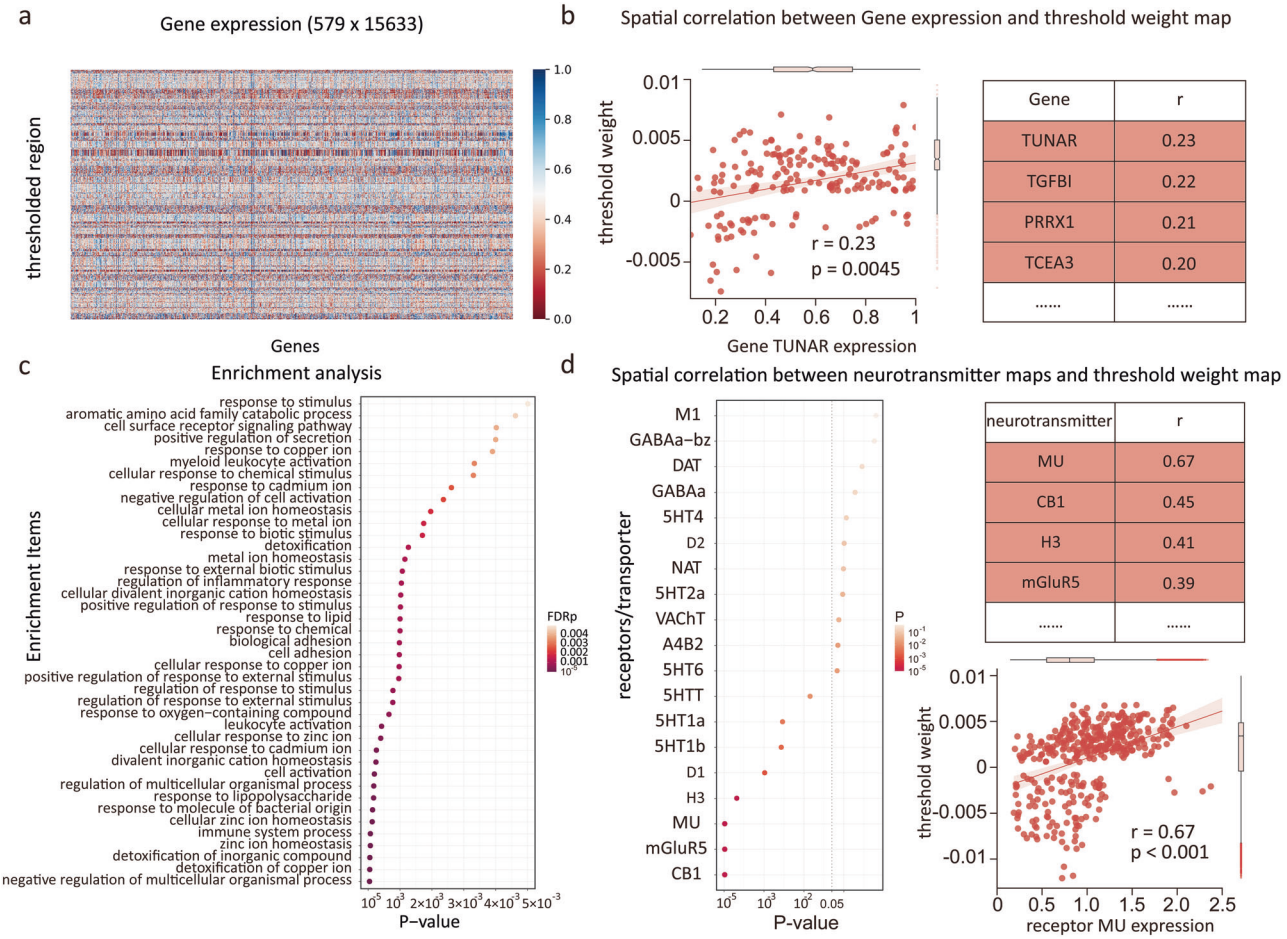

Fig. 5 | Spatial correlation between gene/neurotransmitter map and thresholded map and enrichment analysis. a Normalized gene expression levels in 579 regions. **b** The correlation between the expression profile of each gene and the thresholded map. One representative scatter plot was illustrated with positive correlations. **c** Enrichment analysis. **d** The correlation between each neurotransmitter map and thresholded map. One representative scatter plot was illustrated with positive correlations. Source data are provided as a Supplementary Data file.

brain pattern significantly and positively predicted individual DT ability across both task-based fMRI samples.

Using the neural signature of DT to predict individual creativity from resting-state fMRI

To extend the value of the brain pattern and further generalize its predictive power at the individual level, we use data from resting-state modalities to further extend this work. Resting-state functional connectivity is considered a consistent message that measures the organization of intrinsic function within an individual and varies over time and across individuals. Therefore, we used three large-scale resting-state fMRI samples (SLIM, GBB, and BBP) to predict individuals' DT (i.e., AUT) scores. First, we divided the DT brain pattern in 6 clusters including left AG, right IFG, left MTG, left Precuneus, right Thalamus, right cerebellum as 6 ROIs. Second, we constructed 6×6 symmetric Functional connectivity (FC) matrix with 15 unique edges per participant (see 'Methods' for details). Then, we applied RVR with 15 unique edges as feature to predict creative ratings for each subject on Southwest University Longitudinal Imaging Multimodal (SLIM) with a 10×10-fold cross-validation. The prediction results were shown in Fig. 7b. The distribution of the correlation(r) between the predicted value and the true value in 10×10-fold cross-validations ranged from 0.05 to 0.19 (average $r = 0.15$, $p_{pt} = 0.002$, mean absolute error = 0.76). To identify significant features that reliably contribute to the DT, we conducted bootstrap tests with 10,000 iterations. The functional connectivity between the left AG and left MTG, left AG and left Precuneus, left MTG and right cerebellum significantly predicted individual DT scores (Fig. 7a).

Then, we conducted a validation analysis on Gene-Brain-Behavior (GBB) and BBP samples. Specifically, we calculated the Pearson correlation between functional connectivity (between left AG and left MTG, left AG and left Precuneus, left MTG and right cerebellum) and individual DT scores in GBB and BBP. In the GBB sample, functional connectivity between left AG and left MTG was positively correlated with DT ($r = 0.14$, $p = 0.018$) (Fig. 7c top), whereas functional connectivity between left AG and left Precuneus ($r = 0.08$, $p = 0.16$), as well as left MTG and right cerebellum ($r = 0.02$, $p = 0.74$) were both not significantly correlated with DT. In the BBP sample, we found that functional connectivity between left AG and left MTG was positively correlated with DT ($r = 0.10$, $p = 0.017$) (Fig. 7c bottom), whereas functional connectivity between left AG and left Precuneus ($r = 0.04$, $p = 0.38$), as well as left MTG and right cerebellum ($r = -0.01$, $p = 0.73$) were both not significantly correlated with DT. Taken together, resting-state functional connectivity of some, but not all, regions in the task-based DT brain activity pattern was correlated with individual DT ability.

Discussion

The current study aimed to develop and validate a comprehensive brain profile that captures the essence of DT. This profile demonstrates the potential to predict individual scores of DT, offering practical applications in understanding individual creative thinking. Through the utilization of MVPA, we examined the neural representation of DT across the entire brain, comparing it to control conditions. Notably, these brain features were found to be predominantly distributed within the default, frontoparietal, and limbic networks. Further, through spatial correlation analysis with

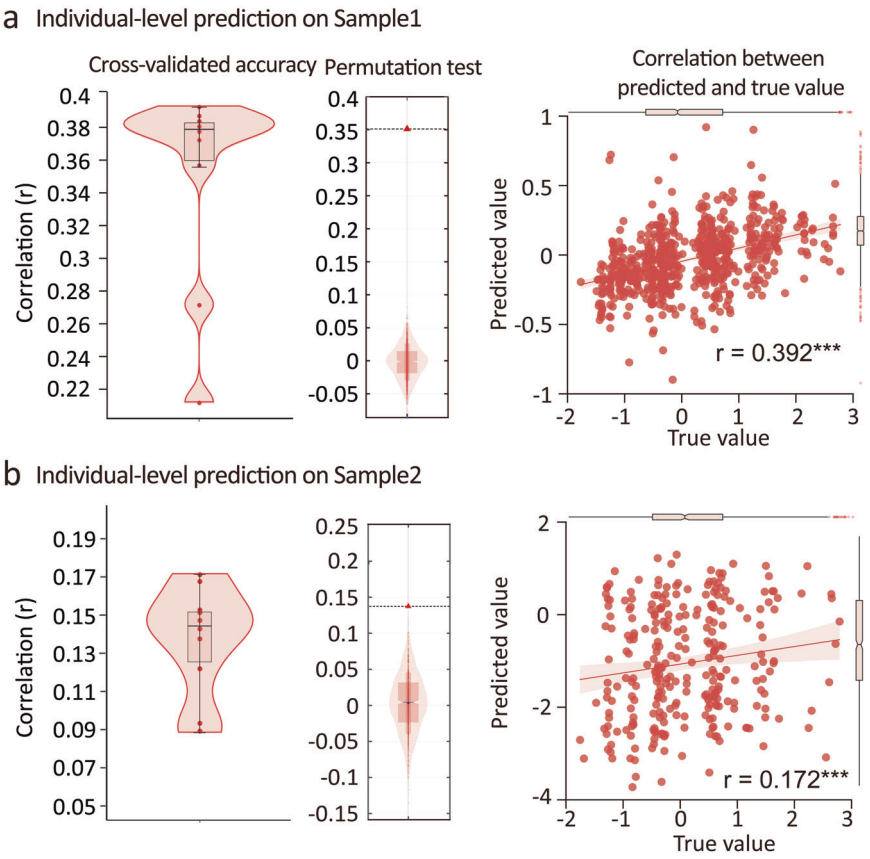

Fig. 6 | DT brain pattern predicts AUT self-rating score. a The distribution of the correlation(*r*) between the predicted value and the true value in 10 × 10-fold cross-validations on sample 1. One representative scatter plot was illustrated. **b** The distribution of the correlation(r) between the predicted value and the true value in 10 × 10-fold cross-validations on sample 2. One representative scatter plot was illustrated. Source data are provided as a Supplementary Data file.

resting-state functional connectivity gradients, we uncovered the organizing principles of the DT brain pattern. We also explained this brain pattern from cognitive and biogenetic perspectives, respectively. The DT brain pattern was associated with higher-order cognitive functions (such as memory, judgment, and reasoning), increased expression levels of genes that influence neurotransmitter release, as well as increased release of neurotransmitters related to mood and reward such as dopamine, MOR, CB_1. Additionally, the features of the DT brain activity pattern were able to predict DT scores at the individual level and demonstrate generalizability across different modalities—task-based activity pattern and resting-state functional connectivity. Collectively, these findings shed light on the neural expression of creative thinking in the human brain, offering insights into its cognitive functioning and biological underpinnings.

We observed that the DT brain pattern was distributed across a broad range of regions, primarily including bilateral DLPFC, bilateral DMPFC, left VLPFC, bilateral ACC, bilateral OFC, left AG, and bilateral thalamus regions. These brain regions are distributed across a wide range of brain networks involved in different cognitive functions, and we first parsed such representational patterns from a cognitive decoding perspective. Our results suggest that DT brain patterns share partial commonalities with many representations of cognitive functions. For instance, free association refers to the process by which an individual spontaneously links one thought, memory, or concept to another related or unrelated thought, memory, or concept without external constraints or control[36], primarily involving the activation of brain regions within DMN[37]. Working memory, as a form of higher-order cognition, is a cognitive system responsible for the sustained attention, monitoring, temporary storage, and manipulation of information[38], and it primarily involves widespread and consistent activation of regions such as the DLPFC, VLPFC, and parietal cortex[39]. Inhibitory control refers to the ability of an individual to suppress or regulate responses when faced with inappropriate or irrelevant distractions, which is a key component of executive functions[40]. This function is mainly associated with the DLPFC, inferior frontal cortex or OFC[40–42], as well as the ACC and posterior parietal cortex[42]. These cognitive abilities partially overlap with the brain patterns associated with DT. The spontaneous cognitive process (free association) is related to enhanced internal connectivity within the DMN, which facilitates associative fluency in creative processes, thereby improving performance on creativity tasks[43]. Working memory contributes to DT through attentional control mechanisms that manage and guide the complex search processes[44]. The inhibitory control system of the prefrontal cortex suppresses spontaneously generated solutions that are rapid/unconscious, ultimately preserving only original ideas [45–47].

When overlapping with large resting-state brain networks, we found that these regions mainly reside within the DMN, the FPCN, and a small portion of the limbic network. The DMN consisting of the MPFC, precuneus, and AG is typically associated with spontaneous thinking, daydreaming, or associative processes[48–50]. During the generation of ideas in DT, the DMN facilitates the production of ideas by supporting a series of associative processes in semantic memory through spontaneous and unconscious recall[51–54]. The FPCN, involving the DLPFC, VLPFC, and dorsomedial thalamus, is typically associated with executive control processes[55–57]. During DT, the FPCN is responsible for evaluating and selecting the generated ideas, filtering out those that are insufficiently novel, and ultimately producing innovative thought[18,58–60]. Additionally, our results indicate that the primary sensory and motor networks play an inhibitory role in the brain's production of DT. Therefore, both the DMN and FPCN are crucial for DT, and their activity is accompanied by a reallocation of resources within the visual network, reducing reliance on external visual information while enhancing internal thinking and imagery [61,62].

However, beyond observing the representation of DT from the perspective of discrete networks, the emergence of resting-state functional connectivity gradients provides a new perspective for understanding it from a continuous standpoint. The principal gradient is generally considered to reflect the global hierarchical structure of brain function, with the DMN that represents high-level/abstract cognitive processes, positioned at one end, and the primary sensory and motor networks at the other[25]. Our findings

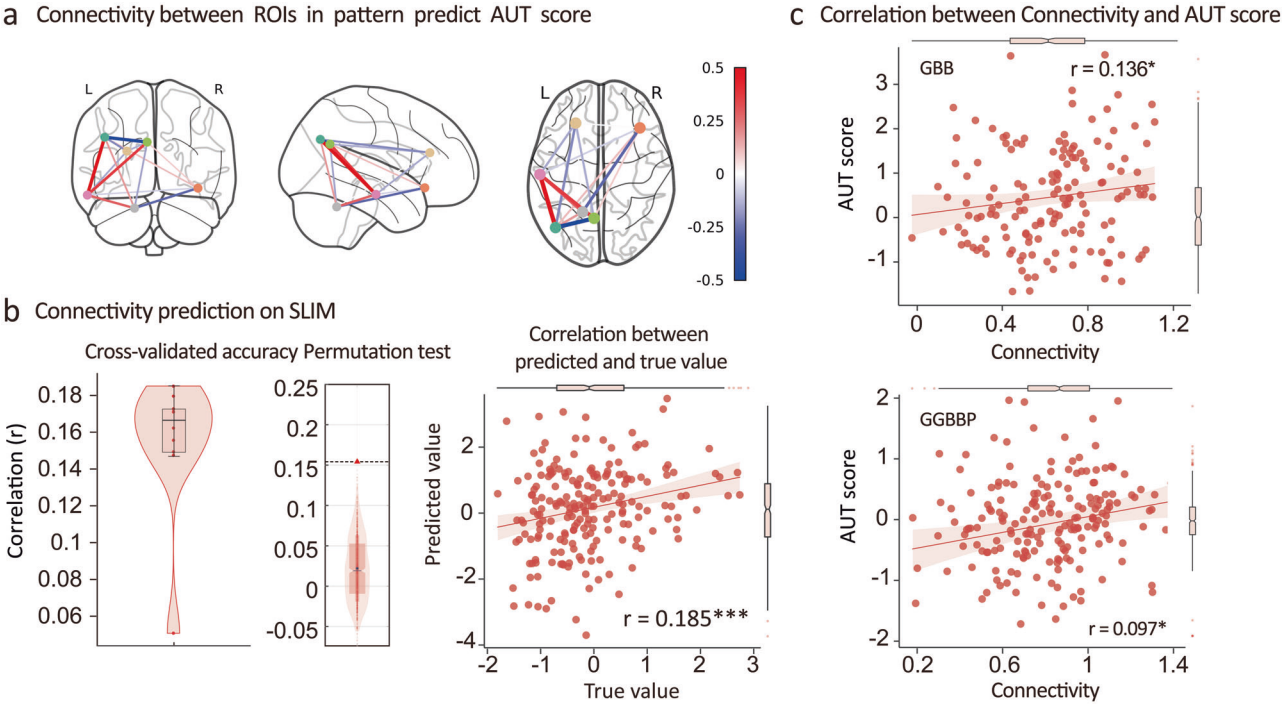

Fig. 7 | Resting-state functional connectivity between DT brain regions predicts AUT score. a The connectivity map shows the feature weight for predicting DT (i.e., AUT score). **b** The distribution of the correlation(r) between the predicted value and the true value in 10 × 10-fold cross-validations on SLIM. One representative scatter plot was illustrated. **c** Correlation between resting-state functional connectivity and DT ability in GBB and BBP. Source data are provided as a Supplementary Data file.

reveal a strong positive correlation between the distribution of brain features associated with DT and the principal gradient, which first highlights the critical role of the DMN in DT. Moreover, this suggests that the neural representation of DT is not distributed in a discrete and unstructured manner across various brain regions but rather organized in a continuous gradient that hierarchically structures brain regions with different functions, forming a unique neural organizational principle for DT. DT likely depends on the dynamic integration of functional regions[20,63], from basic sensory input to high-level cognition. Additionally, DT requires flexible integration and cooperation among these different networks, aligning with research that emphasizes the need for high cognitive flexibility[64–66], which involves rapidly shifting from one idea to another. In summary, we propose that creative thinking involves a broad integration from concrete sensory information to abstract, high-level cognition. The core of creative thinking lies in the distinctive coordination and organizational framework that spans across brain networks, distinguishing it from other high-level cognitive functions.

Next, we explained the DT brain pattern from a biogenetic perspective. We established links between the DT brain pattern and enriched expression of genes involved in the release of the neurotransmitters such as dopamine, MOR, CB_1, H_3, and $mGluR_5$, as well as the negative regulation of multicellular organismal processes, and detoxification of copper ions and inorganic compounds. Negative regulation of multicellular organismal processes (https://www.yeastgenome.org/go/GO:0051241) refers to the process of inhibiting/preventing or reducing the frequency/rate or extent of various activities in multicellular organisms. Excessive accumulation of copper ions with other inorganic compounds can lead to neurological damage, affecting neurotransmitter synthesis/release and messaging processes[67–69]. We, therefore, suggest that negative regulation of multicellular organismal processes and the detoxification of copper ions and other inorganic compounds may affect the overall functioning of the organism, potentially influencing its ability to engage in DT activities or problem-solving. Neurotransmitter release has been linked to creative cognition, and creative drives such as motivation, emotional states, and rewards can influence creative thinking through related neuromodulatory systems[70]. It has been suggested that positive-activating moods with an approach motivation (e.g., happiness) promote creativity[71,72]. In addition to this, many researchers have emphasized the close link between rewards and creativity, as the promise of rewards may facilitate creative thinking and original solutions [73,74].

The dopamine system is involved in various aspects of cognitive function related to reward, addiction, attention, and compulsion, and studies have shown that interactions between the frontal and striatal dopamine pathways can contribute to creative cognition by facilitating flexible processing and sustained-driven creativity[70,75]. Kranz, Kasper, and Lanzenberger[76] made the argument that serotonin serves as an important mediator of the affective, motivational, and cognitive elements of reward representations, and thus the neurotransmitter serotonin has similar value to dopamine in reward processing[70]. Similarly, opioids such as MOR are distributed in the reward centers of the brain and are associated with the regulation of pain, reward, and addictive behaviors[77–79]. Moreover, other studies have mentioned that highly potent cannabis which affects CB_1 receptors may impair DT[80]; H_3 receptors are involved in various cognitive and motor processes[81], play a role in the central nervous system and have been explored as a potential target for cognitive symptoms and impairments[82]; $mGluR_5$ plays an important role in memory and learning processes in the brain[83]. Thus, our findings are consistent with previous studies and provide evidence supporting the link between dopamine release and DT brain patterns from a novel perspective. In addition to this, evidence was also obtained that other neurotransmitters and related gene expression profiles are associated with DT, which may provide a neurobiological explanation of the DT brain pattern.

Finally, the DT brain pattern also predicted individual-level creativity scores well. Meanwhile, the predictive power of brain patterns was further generalized across three large resting-state samples, in addition to the two task-based samples. This suggests that brain pattern not only represents a common basis for neural representations of DT but also captures individual differences in generating creative ideas and problem-solving. Understanding individual differences in DT can help identify individuals who excel in this area, and these assessments, used in the fields of psychology and education, can also be used to develop effective interventions for students to improve their learning experiences and outcomes.

A limitation of the present study was the use of the AUT, although this task is typically used to measure DT (thus better aligning our work with prior DT studies). The traditional AUT suffers from poor reliability, influenced by various factors. This study mitigated individual differences associated with the task itself by making adaptations. With respect to solution duration, participants were instructed to generate a response based on the items provided, without the need to generate as many responses as possible, thus addressing potential changes resulting from a longer solution duration. Additionally, compared to previous AUT administrations, the present study expanded the pool of stimulus words by selecting 80 specific object words (e.g., "umbrella") from an entity noun library as experimental stimuli (K[84]). To ensure the suitability of each object word for idea generation, five trained raters evaluated their appropriateness[85], thus minimizing individual differences arising from the choice of stimulus words.

Although the present study integrated neural, cognitive, and genetic approaches to comprehensively study verbal DT, future studies should apply such integrated fMRI-based approaches to investigate other forms of DT (e.g., visual), as well as convergent thinking which is also important for creativity. Similarly, future studies should utilize such integrated methods to assess creativity across domains (e.g., music, art, science). Indeed, approaches which integrate neuroimaging and biogenetic methods are needed for holistic creativity neuroscience, yet such approaches remain rare in the literature. Additionally, the current study's sample was predominantly female, we encourage future research to include a more balanced sample to enhance generalizability.

In conclusion, the present study has identified a comprehensive neural representation of DT and its organizational principle, which has been validated and generalized across independent samples and various data modalities. Additionally, the DT brain pattern was explained from both cognitive decoding and neurobiological perspectives, as this pattern was positively linked to cognitive abilities (e.g., memory and reasoning), and neurotransmitter release (e.g., dopamine). Taken together, these findings offer substantial evidence for the neural representation and deciphering of DT, enhancing our comprehension of its cognitive significance and underlying biological foundations.

Methods

Task-based fMRI samples

Participant. The task-based fMRI data employed in the current study comes from two independent samples. A total of 57 subjects were recruited in Sample 1 (43 females, mean age = 19.23 years, SD = 0.96, range = 17–22 years). Two subjects were excluded from subsequent analyses due to image abnormalities when normalized to standard space. Thus, 55 subjects within sample 1 were include in the following analysis. Sample 2 has a total 31 participants (20 females, mean age = 19.30 years, SD = 2.49, range = 17–28 years). One subject was excluded from subsequent analyses due to falling asleep during scanning. Thus, 30 subjects were included in the following analyses. All subjects were college students at Southwest University, all were healthy, met MRI safety criteria (e.g., they had no stents or metal implants), and had no history of neurological or psychiatric problems. In accordance with the Declaration of Helsinki, all subjects provided written informed consent prior to participation in the study and were paid for their participation.

Stimuli and paradigm

Sample 1. Subjects performed an adjusted version of the AUT during the fMRI scan (Fig. 1a). The task contains two conditions, the control condition is the general use (GU) condition, which requires subjects to answer what is commonly used for the provided object (an entity), e.g., a map is commonly used for navigation (map->navigation). The DT condition is the novel use (NU) condition, which requires subjects to generate original and unique uses for a given object, e.g., a map can be used to make a necklace (map -> necklace). The procedure consists of 4 sessions, each session includes 20 trials, with 12 NU conditions and 8 GU conditions. Each trial starts with a fixation screen for 2 s. Then the cue for the experimental condition - "novel use" (or "general use") appears on the screen for 4 s, followed by the object (e.g., ring -> ?) and remains on the screen for 12 s, (the "general use" condition has the object on the screen for 4 s), which is called the idea generation period. In this phase, subjects must think about possible responses to a given stimulus (original usage of an everyday object or general use of a given noun). If response comes to mind, the subject is asked to quickly press "1" with the left hand and then write down the response on the paper as quickly as possible (within 6 s), summarizing the response in one phrase (2–3 words). If no response comes to mind, the subject cannot press a key and draws an "X" on the paper when the writing prompt appears. Finally, the "rest" appeared on the screen for 8 s and the subject was asked not to write, to look at the screen and to remain calm. The experimental conditions are presented in random order and total time for the task is about 40 min. After the MRI scan, subjects were asked to recall and refine their responses, and then rate the originality of their responses using a 5-point scale that ranged from 1 ('not original') to 5 ('highly original'). Collecting individuals' ratings of the originality of their answers based on personal meaning can reflect their own creative processes and internal reward mechanisms, revealing their self-perception of creative performance (K[86,87]).

Sample 2. Sample 2 was obtained from[85], in which two conditions NU and GU, consistent with sample 1, were selected for subsequent analysis in this study. The procedure consists of 6 sessions, total 40 NU conditions and 20 GU conditions. As with sample 1, after the MRI scan, subjects were asked to recall and refine their responses, and then rate the originality of their responses using a 5-point scale that ranged from 1 ('not original') to 5 ('highly original').

MRI data acquisition and preprocessing

MRI data acquisition. Whole-brain imaging was acquired on a Siemens 3T Trio scanner (Siemens Medical Systems, Erlangen, Germany) at the Brain Imaging Center, Southwest University. Task fMRI images were acquired using Gradient Echo Type Echo Planar Imaging (GRE-EPI) sequence (TR/TE = 2000 ms/30 ms, FA = 90°, resolution matrix = 64 × 64, FOV = 220 × 220 mm^2, thickness = 3 mm, slices = 32, interslice gap = 1 mm, acquisition voxel size = 3.4 × 3.4 × 4 mm^3). High-resolution three-dimensional T1-weighted structure images were obtained using a Magnetization Prepared Rapid Acquisition Gradient-echo (MPRAGE) sequence (TR/TE = 1900 ms/2.52 ms, FA = 9°, FOV = 256 × 256 mm^2, slices = 176, thickness = 1.0 mm, voxel size = 1 × 1 × 1 mm^3).

MRI data preprocessing. For each of the 4 (6 in sample 2) BOLD (Blood Oxygen Level-Dependent) runs found per subject (across all tasks and sessions), the following preprocessing was performed. First, a reference volume and its skull-stripped version were generated using a custom methodology of fMRIPrep. Head-motion parameters with respect to the BOLD reference (transformation matrices, and six corresponding rotation and translation parameters) are estimated before any spatiotemporal filtering using mcflirt (FSL 6.0.5.1:57b01774, Jenkinson et al., 2002). BOLD runs were slice-time corrected to 0.962 s (0.5 of slice acquisition range 0–1.93 s) using 3dTshift from AFNI (Cox and Hyde 1997, RRID:SCR_005927). The BOLD time-series (including slice-timing correction when applied) were resampled onto their original, native space by applying the transforms to correct for head-motion. These resampled BOLD time-series will be referred to as preprocessed BOLD in original space, or just preprocessed BOLD. The BOLD reference was then co-registered to the T1w reference using mri_coreg (FreeSurfer) followed by flirt (FSL 6.0.5.1:57b01774, Jenkinson and Smith 2001) with the boundary-based registration (Greve and Fischl 2009) cost-function. Co-registration was configured with six degrees of freedom. Several confounding time-series were calculated based on the preprocessed BOLD: framewise displacement (FD), DVARS, and three region-wise global signals. FD was computed using two formulations following Power (absolute sum of relative motions, Power et al. (2014)) and Jenkinson (relative root mean

square displacement between affines, Jenkinson et al. (2002)). FD and DVARS are calculated for each functional run, both using their implementations in Nipype (following the definitions by Power et al., 2014). The three global signals are extracted within the CSF, the WM, and the whole-brain masks. Additionally, a set of physiological regressors were extracted to allow for component-based noise correction (CompCor, Behzadi et al. 2007). Principal components are estimated after high-pass filtering the preprocessed BOLD time-series (using a discrete cosine filter with 128 s cut-off) for the two CompCor variants: temporal (tCompCor) and anatomical (aCompCor). tCompCor components are then calculated from the top 2% variable voxels within the brain mask. For aCompCor, three probabilistic masks (CSF, WM and combined CSF + WM) are generated in anatomical space. The implementation differs from that of Behzadi et al. in that instead of eroding the masks by 2 pixels on BOLD space, the aCompCor masks are subtracted a mask of pixels that likely contain a volume fraction of GM. This mask is obtained by thresholding the corresponding partial volume map at 0.05, and it ensures components are not extracted from voxels containing a minimal fraction of GM. Finally, these masks are resampled into BOLD space and binarized by thresholding at 0.99 (as in the original implementation). Components are also calculated separately within the WM and CSF masks. For each CompCor decomposition, the k components with the largest singular values are retained, such that the retained components' time series are sufficient to explain 50 percent of variance across the nuisance mask (CSF, WM, combined, or temporal). The remaining components are dropped from consideration. The head-motion estimates calculated in the correction step were also placed within the corresponding confounds file. The confound time series derived from head motion estimates and global signals were expanded with the inclusion of temporal derivatives and quadratic terms for each (Satterthwaite et al., 2013). Frames that exceeded a threshold of 0.5 mm FD or 1.5 standardised DVARS were annotated as motion outliers. The BOLD time-series were resampled into standard space, generating a preprocessed BOLD run in MNI152NLin2009cAsym space. First, a reference volume and its skull-stripped version were generated using a custom methodology of fMRIPrep. All resamplings can be performed with a single interpolation step by composing all the pertinent transformations (i.e., head-motion transform matrices, susceptibility distortion correction when available, and co-registrations to anatomical and output spaces). Gridded (volumetric) resamplings were performed using antsApplyTransforms (ANTs), configured with Lanczos interpolation to minimize the smoothing effects of other kernels (Lanczos 1964). Non-gridded (surface) resamplings were performed using mri_vol2surf (FreeSurfer).

First-level fMRI analysis

We conducted two separate GLM (general linear model) analysis in SPM12: subject-level analysis and single-trial analysis in two samples respectively. Subject-level GLM was used to obtain beta images for the Multivariate voxel pattern analysis. The four runs of the stimulation task were concatenated for each subject. The onset of the two conditions (NU and GU) was modeled using a canonical hemodynamic response function. Single-trial analysis was used to obtain beta images for the RVR analysis. To estimate single-trial responses, we conducted a GLM design matrix with separate regressors for each trial with respective onset time. Six head motion parameters (x, y, z, roll, pitch and yaw) are included in the matrix as confounding variables and a high pass filter of 128 s was applied to remove low-frequency drifts.

Multivariate voxel pattern analysis

We applied whole-brain (restricted to a gray matter mask) multivariate machine-learning pattern analysis to obtain a brain activation pattern that best-classified subjects in NU and GU. We used the SVM algorithm using a linear kernel ($C = 1$) implemented in the Interpreting machine learning models in neuroimaging toolbox (https://github.com/cocoanlab/interpret_ml_neuroimaging) with individual beta maps (one condition for each subject) as feature to classify subjects in NU and GU while undergoing fMRI. We performed the classification on sample 1 and sample 2, respectively. Neuroimaging studies are usually based on small number of subjects. Therefore, we used cross-validation (CV) strategies to overcome the loss of generalization due to the small training and testing sample size in the neuroimaging applications. To evaluate the performance, 10 × 10-fold CV procedure on the sample1 and sample2 was conducted respectively. All subjects were randomly assigned to 10 subsamples of 5 or 6 subjects (3 subjects in sample 2). The optimal hyperplane was computed based on the multivariate pattern about 50 participants (27 subjects in sample 2) (training set) and evaluated by the excluded 5 or 6 participants (3 subjects in sample 2) (test set). This procedure was repeated ten times, once for each subsample of the test set. To avoid potential bias in the training-test split, the CV procedure was repeated ten times throughout the study, with each repetition producing a different split, resulting in the prediction performance being averaged to produce a convergent estimate. We evaluated the performance of the SVM models from the following indices: accuracy, sensitivity, specificity, ROC, AUC and the definitions is as follows. Accuracy was defined as the ratio of the correct predictions to the total number of classifications: accuracy = (TP + TN)/(TP + FP + TN + FN). The ROC was also calculated by the one-versus-rest approach, with the parameter sensitivity and specificity denoted by: sensitivity = TP/(TP + FN) and specificity = TN/(TN + FP). Here, TP is the true positive, FP is the false positive, TN is the true negative and FN is the false negative for each label. We also performed a permutation test to estimate the empirical distribution of the classifier accuracy under the null hypothesis. To this end, we tested the SVM classifier with the random labeling and calculated the accuracy of SVM classifier in sample 1 and sample 2 respectively. The permutation test was repeated 5000 times. Classifier performance greater than 95% of the random permutations indicates above-chance accuracy (given an alpha of $p < 0.05$). To test the generalization performance of the two classification models, we performed validation using sample 2 (sample 1) as the validation set. We calculated the dot-product of vectorized activation images in sample 2 (sample 1) with the threshold weights of the model in sample 1 (sample 2). Then the average accuracy, sensitivity, specificity, positive predictively, and the AUC across this repetition were calculated. Bootstrap tests were conducted to provide P-values for voxel weights to threshold the classifier weights for display and interpretation. We constructed 10,000 bootstrap sample sets (with replacement) and ran SVMs on each bootstrap sample. Each bootstrap sample serves as training data for a new model. The hyper-parameters of the model were the same as the original model. Then, two-tailed, 5000 permutation tests were conducted to calculation P-values for each voxel based on the proportion of weights above or below zero. Then we performed FDR multiple comparison correction for the results of permutation test.

DT brain pattern obtained by classifier weights of two samples

Since the model weights obtained on the two samples had a high positive correlation, we combined the weights map of the two samples to obtain the final brain activation pattern that could be classified as specific to novel idea generation. First, we overlap the weights of the classification model trained by two samples separately to gain the common region. Then, we averaged the weight values of the voxels in the common region to obtain the DT brain pattern.

Evaluate the neurobiological validity of the model

To evaluate the neurobiological plausibility and validity of SVM model, we conducted biology-level assessments. The first assessment is evaluating overlaps of the MVPA-based DT brain pattern with large-scale resting-state functional networks. We used the mask that had unique values for seven resting-state functional networks[88]. Then, we calculated the posterior probability of observing the DT brain pattern given each network. Specifically, we calculated the overlap-based similarity separately for positive and negative predictive weights. The second assessment is using a large-scale meta-analytic decoding framework provided by Neurosynth, we can identify the psychological terms associated with DT brain pattern of predictive weights values. We used meta-analytic maps previously generated for various psychological terms and assessed their similarity to the DT brain pattern, implemented in the Neurosynth Python package (https://github.com/

neurosynth/neurosynth/blob/master/neurosynth/analysis/decode.py). Then, it returns a list of the terms with correlation coefficients between the DT brain pattern and the meta-analytic maps. Then, to explore the neural organizational principle of the DT brain pattern, we calculated the Pearson's correlation coefficient between the weights in DT brain pattern (i.e., the β-map) between previously-identified gradients. The group-level (averaged across participants) first ten gradients maps was accessed via the neuromaps (https://netneurolab.github.io/neuromaps/)[89]. Firstly, we assigned the DT brain pattern to the gradient map. Then, the Pearson's correlation between the β values and the gradient values across the overlapping regions was calculated. The statistical significance of association was assessed using "spin tests" (as detailed below in the "null model" section).

Spatial correlation between gene expression and DT brain pattern

Microarray expression data were obtained from six post-mortem brains provided by the Allen Human Brain Atlas (AHBA; http://human.brain-map.org/[90]). Preprocessing was performed using the abagen toolbox (https://github.com/netneurolab/abagen[91]). Each human brain tissue sample was preprocessed according to a recommended pipeline with default settings. We assigned all tissue samples from Allen Human Brain Atlas to DT brain pattern regions, resulting in expression level maps for 15,633 gene covering 574 regions within DT brain pattern. Samples were assigned to brain regions in the provided DT brain pattern region if their MNI coordinates were within 2 mm of a given parcel (the DT brain pattern native space is 2 mm). Then, we normalized gene expression levels across probes within the sample and across samples within a subject. This preprocessing produced a group-level (averaged across donors) gene expression profile of the 574 regions within DT brain pattern. To explore whether DT brain pattern is associated with gene transcriptional profiles, we calculated the Pearson's correlation coefficient between the weights in DT brain pattern (i.e., the β-map) and the preprocessed expression profile of each gene in the microarray. Firstly, the DT brain pattern β-map was aligned to the 574 regions as described above. Then, the Pearson's correlation between the β-map values and the gene expression values across the 574 overlapping regions was calculated. The statistical significance of association was assessed using "spin tests" (as detailed in the next section). We then arranged all genes in descending order according to the significance level of the correlation coefficients, starting with the genes with the most significant positive correlation to those with the most significant negative correlation. Subsequently, we uploaded the sequenced gene sets to the Gene Ontology enrichment analysis and visualization tool (GOrilla, http://cbl-gorilla.cs.technion.ac.il/)[92]: (i) a threshold of $P < 10^{-5}$ in the advanced parameter settings; and (ii) q-value < 0.05 in Benjamini–Hochberg FDR corrections.

Spatial correlation between neurotransmitter expression and DT brain pattern

We used neuromaps (https://netneurolab.github.io/neuromaps/[89]); to access volumetric PET images previously collected for 19 different neurotransmitter receptors and transporters across 9 different neurotransmitter systems (Bedard et al. [93–95], Ding et al. [96–109]). To protect patient privacy, individual subject maps were averaged across studies prior to sharing. Each study, associated receptor/transporter, tracer, number of healthy subjects, age and references, and complete methodological details can be found in ref.[110]. The Pearson's correlation between the DT brain pattern β-map and the receptors/transporters map was calculated. Then, the statistical significance of the association is assessed using a "spin test" (as detailed in the next section).

Null model

Spatial autocorrelation-preserving permutation tests were used to assess the statistical significance of associations across brain regions, called "spin tests". Specifically, we choose for each parcel the vertex closest to its center of mass on the spherical projection of the fsaverage surface. We then rotate the coordinates of these centers of mass and reassign the values of the closest rotated parcels to each parcel. This procedure is repeated 10,000 times. These processes were implemented in neuromaps (https://netneurolab.github.io/neuromaps/[89]).

Relevance vector regression analysis within DT brain pattern

We applied RVR to examine the effectiveness of the DT brain pattern as a brain activation pattern that is specific to original idea generation, implemented in the Pattern_Regression_Matlab (https://github.com/ZaixuCui/Pattern_Regression_Matlab). First, we use the positive activation region within the DT brain pattern as ROI. Then, the single-trial beta maps (only NU condition for each subject) as feature to predict originality ratings for DT responses. RVR is a sparse kernel multivariate regression method that uses Bayesian inference to obtain analytic solutions that generalize well and provide inference at low computational cost. RVR has no specific algorithm parameters and does not require additional computational resources to estimate the best specific algorithm parameters. Sample 1 had a total of 2047 NU trials and sample 2 had a total of 846 NU trials. To evaluate the performance, 10 × 10-fold CV procedure on the sapmle1 and sample2 was conducted respectively. All trials were randomly assigned to 10 subsamples, ninefolds were used as the training set, and the remaining fold was used as the testing set. We included gender, age, and head movement as control variables in the analysis. This procedure was repeated ten times, once for each subsample of the test set. Pearson correlation coefficients and mean absolute errors between predicted and actual scores were calculated to provide a final estimate of prediction performance. Prediction performance greater than 95% of the random permutations indicates above-chance accuracy (given an alpha of $p < 0.05$).

Large-scale resting-state fMRI samples

Participants. The resting-state fMRI data employed in current study comes from three independent datasets. The main dataset comes from the SLIM project. The validation datasets included data from the GBB project and Behavioral Brain Research Project of Chinese Personality (BBP). All projects were approved by the Southwest University Brain Imaging Center Institutional Review Board. In accordance with the Declaration of Helsinki, all subjects provided written informed consent prior to participation in the study. The recruiting program and exclusion procedures of participants in SLIM and GBB have been described in detail elsewhere[111,112]. After matching with behavioral data, the present study included 410 undergraduates from SLIM (233 females, mean age = 20.01 years, SD = 1.24, range = 17–27 years), 304 undergraduates from GBB (218 females, mean age = 19.70 years, SD = 1.73, range = 17–26 years). A total of 804 undergraduates from the BBP were recruited, after excluding 31 participants with excessive head motion (mean FD (Jenkinson) greater than ±0.2 mm) and matching with behavioral data, the present study included 600 undergraduates from BBP (412 females, mean age = 20.7 years, SD = 0.99, range = 17–27 years).

MRI data acquisition and preprocessing

MRI data acquisition. The resting-state fMRI data sets were collected using the same scanner at the Brain Imaging Center of Southwest University. The SLIM and GBB datasets used the same scanning sequence as task-based fMRI data. The BBP images were acquired using Gradient Echo Type Echo Planar Imaging (GRE-EPI) sequence (TR/TE = 2000 ms/30 ms, FA = 90°, resolution matrix = 112 × 112, FOV = 224 × 224 mm^2, thickness = 2 mm, slices = 62, interslice gap = 0.3 mm, acquisition voxel size = 2 × 2 × 2 mm^3). High-resolution three-dimensional T1-weighted structure images were obtained using a MPRAGE sequence (TR/TE = 2530 ms/2.98 ms, FA = 7°, FOV = 224 × 256 mm^2, resolution matrix = 448 × 512, slices = 192, thickness = 1.0 mm, inversion time = 1100 ms, voxel size = 0.5 × 0.5 × 1 mm^3).

MRI data preprocessing. Resting-state fMRI data from the different data sets were preprocessed independently. The preprocessing performed for SLIM and GBB datasets using the fMRIPrep default pipeline that is same as task-based data preprocessing. BBP datasets preprocessing using SPM8 (http://www.fil.ion.ucl.ac.uk/spm) and the Data Processing

& Analysis of Brain Imaging toolbox (DPABI)[113]. We firstly removed the first 10 EPI scans to suppress the equilibration effect, and performed slice timing correction and realignment of the remaining scans. The functional images were then normalized to a standard template (Montreal Neurological Institute) and resampled to $3 \times 3 \times 3\ mm^3$. A Friston 24-parameter model was used to regress nuisance signals including white matter, cerebrospinal fluid, head motion parameters, and their derivatives to control for the potential influence of physiological artifacts. We further implemented data scrubbing to better address head motion concerns. Bad time points were regressed, defined as volumes with frame displacement (FD) power > 0.2 mm, as well as the two succeeding volumes and the one preceding volume to reduce the spillover effect of head motion. In addition, since the BOLD signal exhibits low-frequency drift, linear trends were also used as regressors. Next, we performed spatial smoothing with a 4 mm full-width half-maximum Gaussian kernel and band-pass temporal filtering (0.01–0.1 Hz). Finally, we did not perform global signal regression (GSR) considering several issues: the use of GSR has been controversial because the global signal also includes BOLD fluctuations associated with neurons, especially when these fluctuations are strong and widespread throughout the brain. If the global signal is removed, these neuron-related fluctuations will be removed. GSR introduces a negative bias in the estimated BOLD response, reducing the positive BOLD response and artificially creating a negative response or "deactivation". Again, the overall effect of GSR in measuring correlation is to force the average correlation across the brain to be zero. GSR may artificially introduce anti-correlations between brain regions that would otherwise not exhibit significant correlations.

Behavioral AUT

To be as consistent as possible with the task-based fMRI, we used behavioral AUT to assess participants' creativity. The AUT[114] is a commonly used measure of DT ability used to assess participants' creativity. In this study, two items commonly used or encountered by Chinese people were provided, namely a can and a brick. Participants were asked to imagine and write down a novel use for each item. The instructions were as follows: "Cans (or bricks) have many unusual USES. In the blanks below, write down the interesting and unusual USES you can imagine. You can think of other people's unexpected uses; the more your ideas, the better; the more novel, the better." AUT scores measure three components: fluency, flexibility, and originality. Fluency refers to the number of meaningful and relevant responses, related to the ability to generate and consider other possibilities. Flexibility refers to the number of responses in different categories, reflecting an individual's ability to switch between conceptual domains. Originality refers to the originality of the answer, thereby providing an index of the response's creative quality, using a 1–5 scale (1 = not creative at all; 5 = very creative)[115,116]. The assessment process was conducted separately by different raters in SLIM, GBB and BBP. In this study, we transformed the scores in every dimension into Z scores within each sample, and the total score for creativity (sum of fluency, flexibility, and originality scores)[117,118] was used as the final creativity score, for each dimension was highly correlated with the total score for creativity, as well as with each other.

Functional network construction on SLIM

The DT brain pattern can be divided into six clusters by the peak values, namely 1. left AG, 2. bilateral OFC, 3. left MTG/ITG, 4. left Precuneus, 5. bilateral PFC/ACC/Thalamus, 6. right cerebellum. These six clusters were treated as nodes in the analysis. A representative time series of each node for everyone was obtained by averaging the time series of all voxels in it. The Pearson correlation of the time courses between each node pair was calculated and then a Fisher Z-transform was performed to improve normality, resulting in a 6×6 symmetric FC matrix with 15 unique edges per participant.

Relevance vector regression analysis on SLIM

We applied RVR to examine the effectiveness of the MVPA-based DT brain pattern as a brain activation pattern that is specific to original idea generation, implemented in the Pattern_Regression_Matlab (https://github.com/ZaixuCui/Pattern_Regression_Matlab) with functional connectivity within biomarker (15 unique edges) as feature to predict individual creativity ratings for each subject on SLIM. To evaluate the performance, 10×10-fold CV procedure was conducted. All subjects were randomly assigned to 10 subsamples, ninefolds were used as the training set, and the remaining fold was used as the testing set. We included gender, age, and head movement as control variables in the analysis. This procedure was repeated ten times, once for each subsample of the test set. Pearson correlation coefficients and mean absolute errors between predicted and actual scores were calculated to provide a final estimate of prediction performance. Prediction performance greater than 95% of the random permutations indicates above-chance accuracy (given an alpha of $p < 0.05$). Bootstrap tests were conducted to provide P-values for edge weights to threshold the predictive weights for display and interpretation. We constructed 10,000 bootstrap sample sets (with replacement). Two-tailed, 1000 permutation test were conducted to calculation P-values for each voxel based on the proportion of weights above or below zero. Then we performed FDR multiple comparison correction for the results of permutation test.

Correlation analysis on GBB and BBP

We applied Pearson correlation to examine the effectiveness of the functional connectivity within the DT brain pattern as feature that significantly predicts individual creative ability. Specifically, we conducted the Pearson correlation between functional connectivity (between left AG and left MTG/ITG, left AG and left Precuneus, left MTG/ITG and right cerebellum) and individual DT scores on GBB and BBP.

Statistics and reproducibility

All statistical tests used, sample sizes, and the number of replicates are described in the corresponding methods.

Reporting summary

Further information on research design is available in the Nature Portfolio Reporting Summary linked to this article.

Data availability

The data and material used in this study are available from the corresponding author upon reasonable request. The source data behind the figures in the paper can be found in Supplementary Data 1.

Received: 7 April 2024; Accepted: 2 October 2024;
Published online: 15 October 2024

References

1. Barbot, B., Hass, R. W. & Reiter-Palmon, R. Creativity assessment in psychological research:(Re) setting the standards. *Psychol. Aesthet. Creat. Arts* **13**, 233 (2019).
2. Sun, M., Wang, M. & Wegerif, R. Effects of divergent thinking training on students' scientific creativity: the impact of individual creative potential and domain knowledge. *Think. Skills Creat.* **37**, 100682 (2020).
3. Akbari Chermahini, S. & Hommel, B. Creative mood swings: divergent and convergent thinking affect mood in opposite ways. *Psychol. Res.* **76**, 634–640 (2012).
4. Guilford, J. P. Measurement and creativity. *Theory Pract.* **5**, 185–189 (1966).
5. Kim, K. H. Meta-analyses of the relationship of creative achievement to both IQ and divergent thinking test scores. *J. Creat. Behav.* **42**, 106–130 (2008).
6. Plucker, J. A. Is the proof in the pudding? Reanalyses of Torrance's (1958 to present) longitudinal data. *Creat. Res. J.* **12**, 103–114 (1999).
7. Runco, M. A. & Acar, S. Do tests of divergent thinking have an experiential bias? *Psychol. Aesthet. Creat. Arts* **4**, 144 (2010).

8. Abraham, A. et al. Creativity and the brain: uncovering the neural signature of conceptual expansion. *Neuropsychologia* **50**, 1906–1917 (2012).
9. Fink, A. et al. The creative brain: Investigation of brain activity during creative problem solving by means of EEG and fMRI. *Hum. Brain Mapp.* **30**, 734–748 (2009).
10. Fink, A. et al. Enhancing creativity by means of cognitive stimulation: evidence from an fMRI study. *NeuroImage* **52**, 1687–1695 (2010).
11. Howard-Jones, P. A., Blakemore, S.-J., Samuel, E. A., Summers, I. R. & Claxton, G. Semantic divergence and creative story generation: an fMRI investigation. *Cogn. Brain Res.* **25**, 240–250 (2005).
12. Kleibeuker, S. W., Koolschijn, P. C. M., Jolles, D. D., De Dreu, C. K. & Crone, E. A. The neural coding of creative idea generation across adolescence and early adulthood. *Front. Hum. Neurosci.* **7**, 905 (2013).
13. Mashal, N., Faust, M., Hendler, T. & Jung-Beeman, M. An fMRI investigation of the neural correlates underlying the processing of novel metaphoric expressions. *Brain Lang.* **100**, 115–126 (2007).
14. Bekhtereva, N. et al. Study of the brain organization of creativity: II. Positron-emission tomography data. *Hum. Physiol.* **26**, 516–522 (2000).
15. Benedek, M., Jauk, E., Sommer, M., Arendasy, M. & Neubauer, A. C. Intelligence, creativity, and cognitive control: The common and differential involvement of executive functions in intelligence and creativity. *Intelligence* **46**, 73–83 (2014).
16. Green, A. E., Kraemer, D. J., Fugelsang, J. A., Gray, J. R. & Dunbar, K. N. Neural correlates of creativity in analogical reasoning. *J. Exp. Psychol. Learn. Mem. Cogn.* **38**, 264 (2012).
17. Kenett, Y. N. et al. Flexibility of thought in high creative individuals represented by percolation analysis. *Proc. Natl Acad. Sci.* **115**, 867–872 (2018).
18. Nusbaum, E. C. & Silvia, P. J. Are intelligence and creativity really so different?: Fluid intelligence, executive processes, and strategy use in divergent thinking. *Intelligence* **39**, 36–45 (2011).
19. Sowden, P. T., Pringle, A. & Gabora, L. The shifting sands of creative thinking: connections to dual-process theory. *Think. Reason.* **21**, 40–60 (2015).
20. Beaty, R. E., Silvia, P. J., Nusbaum, E. C., Jauk, E. & Benedek, M. The roles of associative and executive processes in creative cognition. *Mem. Cogn.* **42**, 1186–1197 (2014).
21. Beaty, R. E., Benedek, M., Barry Kaufman, S. & Silvia, P. J. Default and executive network coupling supports creative idea production. *Sci. Rep.* **5**, 10964 (2015).
22. Beaty, R. E., Benedek, M., Silvia, P. J. & Schacter, D. L. Creative cognition and brain network dynamics. *Trends Cogn. Sci.* **20**, 87–95 (2016).
23. Christensen, A. P., Benedek, M., Silvia, P., & Beaty, R. *Executive and Default Network Connectivity Reflects Conceptual Interference during Creative Imagery Generation* PsyArXiv. https://doi.org/10.31234/osf.io/n438d (2019).
24. Van Essen, D. C. & Glasser, M. F. Parcellating cerebral cortex: how invasive animal studies inform noninvasive mapmaking in humans. *Neuron* **99**, 640–663 (2018).
25. Margulies, D. S. et al. Situating the default-mode network along a principal gradient of macroscale cortical organization. *Proc. Natl Acad. Sci.* **113**, 12574–12579 (2016).
26. Poldrack, R. A. Inferring mental states from neuroimaging data: from reverse inference to large-scale decoding. *Neuron* **72**, 692–697 (2011).
27. Colantuoni, C. et al. Temporal dynamics and genetic control of transcription in the human prefrontal cortex. *Nature* **478**, 519–523 (2011).
28. Douet, V., Chang, L., Cloak, C. & Ernst, T. Genetic influences on brain developmental trajectories on neuroimaging studies: from infancy to young adulthood. *Brain Imaging Behav.* **8**, 234–250 (2014).
29. Levitt, P., Harvey, J. A., Friedman, E., Simansky, K. & Murphy, E. H. New evidence for neurotransmitter influences on brain development. *Trends Neurosci.* **20**, 269–274 (1997).
30. Bogdan, R. et al. Imaging genetics and genomics in psychiatry: a critical review of progress and potential. *Biol. Psychiatry* **82**, 165–175 (2017).
31. Orwig, W. et al. Cortical networks of creative ability trace gene expression profiles of synaptic plasticity in the human brain. *Front. Hum. Neurosci.* **15**, 694274 (2021).
32. Kamitani, Y. & Tong, F. Decoding the visual and subjective contents of the human brain. *Nat. Neurosci.* **8**, 679–685 (2005).
33. Kragel, P. A., Koban, L., Barrett, L. F. & Wager, T. D. Representation, pattern information, and brain signatures: from neurons to neuroimaging. *Neuron* **99**, 257–273 (2018).
34. Arnatkevičiūtė, A., Fulcher, B. D. & Fornito, A. A practical guide to linking brain-wide gene expression and neuroimaging data. *NeuroImage* **189**, 353–367 (2019).
35. Burt, J. B., Helmer, M., Shinn, M., Anticevic, A. & Murray, J. D. Generative modeling of brain maps with spatial autocorrelation. *NeuroImage* **220**, 117038 (2020).
36. Nelson, D. L., McEvoy, C. L. & Dennis, S. What is free association and what does it measure? *Mem. Cogn.* **28**, 887–899 (2000).
37. Smallwood, J. et al. The default mode network in cognition: a topographical perspective. *Nat. Rev. Neurosci.* **22**, 503–513 (2021).
38. Baddeley, A. Working memory. *Science* **255**, 556–559 (1992).
39. Owen, A. M., McMillan, K. M., Laird, A. R. & Bullmore, E. N-back working memory paradigm: a meta-analysis of normative functional neuroimaging studies. *Hum. Brain Mapp.* **25**, 46–59 (2005).
40. Munakata, Y. et al. A unified framework for inhibitory control. *Trends Cogn. Sci.* **15**, 453–459 (2011).
41. Aron, A. R., Robbins, T. W. & Poldrack, R. A. Inhibition and the right inferior frontal cortex. *Trends Cogn. Sci.* **8**, 170–177 (2004).
42. Nee, D. E., Wager, T. D. & Jonides, J. Interference resolution: insights from a meta-analysis of neuroimaging tasks. *Cogn. Affect. Behav. Neurosci.* **7**, 1–17 (2007).
43. Marron, T. R., Berant, E., Axelrod, V. & Faust, M. Spontaneous cognition and its relationship to human creativity: a functional connectivity study involving a chain free association task. *NeuroImage* **220**, 117064 (2020).
44. Gerver, C. R., Griffin, J. W., Dennis, N. A., & Beaty, R. E. Memory and creativity: a meta-analytic examination of the relationship between memory systems and creative cognition. *Psychon. Bull. Rev.* **30**, 2116–2154 (2023).
45. Camarda, A. et al. Do we need inhibitory control to be creative? Evidence from a dual-task paradigm. *Psychol. Aesthet. Creat. Arts* **12**, 351 (2018).
46. Cassotti, M., Agogué, M., Camarda, A., Houdé, O. & Borst, G. Inhibitory control as a core process of creative problem solving and idea generation from childhood to adulthood. *New Dir. Child Adolesc. Dev.* **2016**, 61–72 (2016).
47. Chrysikou, E. G. Creativity in and out of (cognitive) control. *Curr. Opin. Behav. Sci.* **27**, 94–99 (2019).
48. Buckner, R. L., Andrews-Hanna, J. R. & Schacter, D. L. The brain's default network: anatomy, function, and relevance to disease. *Ann. N. Y. Acad. Sci.* **1124**, 1–38 (2008).
49. Fox, K. C. & Beaty, R. E. Mind-wandering as creative thinking: neural, psychological, and theoretical considerations. *Curr. Opin. Behav. Sci.* **27**, 123–130 (2019).
50. Andrews-Hanna, J. R., Smallwood, J. & Spreng, R. N. The default network and self-generated thought: Component processes, dynamic control, and clinical relevance. *Ann. N. Y. Acad. Sci.* **1316**, 29–52 (2014).
51. Shi, L. et al. Large-scale brain network connectivity underlying creativity in resting-state and task fMRI: cooperation between

default network and frontal-parietal network. *Biol. Psychol.* **135**, 102–111 (2018).
52. Bashwiner, D. M., Wertz, C. J., Flores, R. A. & Jung, R. E. Musical creativity "revealed" in brain structure: interplay between motor, default mode and limbic networks. *Sci. Rep.* **6**, 1–8 (2016).
53. Beaty, R. E. et al. Default network contributions to episodic and semantic processing during divergent creative thinking: a representational similarity analysis. *NeuroImage* **209**, 116499 (2020).
54. Marron, T. R. et al. Chain free association, creativity, and the default mode network. *Neuropsychologia* **118**, 40–58 (2018).
55. Shen, K. K. et al. Structural core of the executive control network: a high angular resolution diffusion MRI study. *Hum. Brain Mapp.* **41**, 1226–1236 (2020).
56. Niendam, T. A. et al. Meta-analytic evidence for a superordinate cognitive control network subserving diverse executive functions. *Cogn. Affect. Behav. Neurosci.* **12**, 241–268 (2012).
57. Seeley, W. W. et al. Dissociable intrinsic connectivity networks for salience processing and executive control. *J. Neurosci.* **27**, 2349–2356 (2007).
58. Beaty, R. E. & Silvia, P. J. Why do ideas get more creative across time? An executive interpretation of the serial order effect in divergent thinking tasks. *Psychol. Aesthet. Creat. Arts* **6**, 309 (2012).
59. Beaty, R. E. & Silvia, P. J. Metaphorically speaking: cognitive abilities and the production of figurative language. *Mem. Cogn.* **41**, 255–267 (2013).
60. Gilhooly, K. J., Fioratou, E., Anthony, S. H. & Wynn, V. Divergent thinking: strategies and executive involvement in generating novel uses for familiar objects. *Br. J. Psychol.* **98**, 611–625 (2007).
61. Shi, L. et al. Brain entropy is associated with divergent thinking. *Cereb. Cortex* **30**, 708–717 (2020).
62. Heinonen, J. et al. Default mode and executive networks areas: association with the serial order in divergent thinking. *PLoS ONE* **11**, e0162234 (2016).
63. Silvia, P. J., Beaty, R. E. & Nusbaum, E. C. Verbal fluency and creativity: general and specific contributions of broad retrieval ability (Gr) factors to divergent thinking. *Intelligence* **41**, 328–340 (2013).
64. Wu, Y. & Koutstaal, W. Charting the contributions of cognitive flexibility to creativity: Self-guided transitions as a process-based index of creativity-related adaptivity. *PLoS ONE* **15**, e0234473 (2020).
65. Zabelina, D. L. & Robinson, M. D. Creativity as flexible cognitive control. *Psychol. Aesthet. Creat. Arts* **4**, 136 (2010).
66. Preiss, D. D. Metacognition, mind wandering, and cognitive flexibility: understanding creativity. *J. Intell.* **10**, 69 (2022).
67. Wang, M. et al. Specific recognition, intracellular assay and detoxification of fluorescent curcumin derivative for copper ions. *J. Hazard. Mater.* **420**, 126490 (2021).
68. Algov, I., Feiertag, A., Shikler, R. & Alfonta, L. Sensitive enzymatic determination of neurotransmitters in artificial sweat. *Biosens. Bioelectron.* **210**, 114264 (2022).
69. Nam, E., Nam, G., & Lim, M. H. *Synaptic Copper, Amyloid-β, and Neurotransmitters in Alzheimer's Disease* (ACS Publications, 2019).
70. Boot, N., Baas, M., van Gaal, S., Cools, R. & De Dreu, C. K. Creative cognition and dopaminergic modulation of fronto-striatal networks: Integrative review and research agenda. *Neurosci. Biobehav. Rev.* **78**, 13–23 (2017).
71. Lin, W.-L., Tsai, P.-H., Lin, H.-Y. & Chen, H.-C. How does emotion influence different creative performances? The mediating role of cognitive flexibility. *Cogn. Emot.* **28**, 834–844 (2014).
72. Baas, M., De Dreu, C. K. & Nijstad, B. A. A meta-analysis of 25 years of mood-creativity research: Hedonic tone, activation, or regulatory focus? *Psychol. Bull.* **134**, 779 (2008).
73. Volf, N. & Tarasova, I. The influence of reward on the performance of verbal creative tasks: behavioral and EEG effects. *Hum. Physiol.* **39**, 302–308 (2013).
74. Muhle-Karbe, P. S. & Krebs, R. M. On the influence of reward on action-effect binding. *Front. Psychol.* **3**, 450 (2012).
75. Zabelina, D. L., Colzato, L., Beeman, M. & Hommel, B. Dopamine and the creative mind: Individual differences in creativity are predicted by interactions between dopamine genes DAT and COMT. *PLoS ONE* **11**, e0146768 (2016).
76. Kranz, G., Kasper, S. & Lanzenberger, R. Reward and the serotonergic system. *Neuroscience* **166**, 1023–1035 (2010).
77. Le Merrer, J., Becker, J. A., Befort, K. & Kieffer, B. L. Reward processing by the opioid system in the brain. *Physiol. Rev.* **89**, 1379–1412 (2009).
78. Nummenmaa, L. et al. μ-opioid receptor system mediates reward processing in humans. *Nat. Commun.* **9**, 1500 (2018).
79. Severino, A. L. et al. μ-Opioid receptors on distinct neuronal populations mediate different aspects of opioid reward-related behaviors. *eNeuro* **7**, ENEURO.0146–20.2020 (2020).
80. Kowal, M. A. et al. Cannabis and creativity: highly potent cannabis impairs divergent thinking in regular cannabis users. *Psychopharmacology* **232**, 1123–1134 (2015).
81. Vohora, D. & Bhowmik, M. Histamine H3 receptor antagonists/inverse agonists on cognitive and motor processes: relevance to Alzheimer's disease, ADHD, schizophrenia, and drug abuse. *Front. Syst. Neurosci.* **6**, 72 (2012).
82. Sadek, B., Saad, A., Sadeq, A., Jalal, F. & Stark, H. Histamine H3 receptor as a potential target for cognitive symptoms in neuropsychiatric diseases. *Behav. Brain Res.* **312**, 415–430 (2016).
83. Abd-Elrahman, K. S. & Ferguson, S. S. Noncanonical metabotropic glutamate receptor 5 signaling in Alzheimer's disease. *Annu. Rev. Pharmacol. Toxicol.* **62**, 235–254 (2022).
84. Ding, K. et al. Recognizing ideas generated in a creative thinking task: effect of the subjective novelty. *Curr. Psychol.* **42**, 529–541 (2021).
85. Chen, Q. et al. Common brain activation and connectivity patterns supporting the generation of creative uses and creative metaphors. *Neuropsychologia* **181**, 108487 (2023).
86. Ding, K., He, R., Wang, X., Chen, Q. & Kenett, Y. N. Recognizing ideas generated in a creative task: the roles of the hippocampus and medial prefrontal cortex in facilitating self-generated learning. *Cereb. Cortex* **34**, bhae219 (2024).
87. Madore, K. P., Thakral, P. P., Beaty, R. E., Addis, D. R. & Schacter, D. L. Neural mechanisms of episodic retrieval support divergent creative thinking. *Cereb. Cortex* **29**, 150–166 (2019).
88. Yeo, B. T. et al. The organization of the human cerebral cortex estimated by intrinsic functional connectivity. *J. Neurophysiol.* **106**, 1125–1165 (2011).
89. Markello, R. D. et al. Neuromaps: structural and functional interpretation of brain maps. *Nat. Methods* **19**, 1472–1479 (2022).
90. Hawrylycz, M. J. et al. An anatomically comprehensive atlas of the adult human brain transcriptome. *Nature* **489**, 391–399 (2012).
91. Markello, R. D. et al. Standardizing workflows in imaging transcriptomics with the abagen toolbox. *eLife* **10**, e72129 (2021).
92. Eden, E., Navon, R., Steinfeld, I., Lipson, D. & Yakhini, Z. GOrilla: a tool for discovery and visualization of enriched GO terms in ranked gene lists. *BMC Bioinform.* **10**, 48 (2009).
93. Bedard, M.-A. et al. Brain cholinergic alterations in idiopathic REM sleep behaviour disorder: a PET imaging study with 18F-FEOBV. *Sleep. Med.* **58**, 35–41 (2019).
94. Beliveau, V. et al. A high-resolution in vivo atlas of the human brain's serotonin system. *J. Neurosci.* **37**, 120–128 (2017).
95. Aghourian, M. et al. Quantification of brain cholinergic denervation in Alzheimer's disease using PET imaging with [18F]-FEOBV. *Mol. Psychiatry* **22**, 1531–1538 (2017).
96. Ding, Y. S. et al. PET imaging of the effects of age and cocaine on the norepinephrine transporter in the human brain using (S, S)-[11C] O-methylreboxetine and HRRT. *Synapse* **64**, 30–38 (2010).

97. DuBois, J. M. et al. Characterization of age/sex and the regional distribution of mglur5 availability in the healthy human brain measured by high-resolution [11 c] abp688 pet. *Eur. J. Nucl. Med. Mol. Imaging* **43**, 152–162 (2016).
98. Dukart, J. et al. Cerebral blood flow predicts differential neurotransmitter activity. *Sci. Rep.* **8**, 4074 (2018).
99. Gallezot, J.-D. et al. Kinetic modeling of the serotonin 5-HT1B receptor radioligand [11C] P943 in humans. *J. Cereb. Blood Flow. Metab.* **30**, 196–210 (2010).
100. Hillmer, A. T. et al. Imaging of cerebral α4β2* nicotinic acetylcholine receptors with (−)-[18F] Flubatine PET: Implementation of bolus plus constant infusion and sensitivity to acetylcholine in human brain. *NeuroImage* **141**, 71–80 (2016).
101. Kaller, S. et al. Test–retest measurements of dopamine d 1-type receptors using simultaneous pet/mri imaging. *Eur. J. Nucl. Med. Mol. Imaging* **44**, 1025–1032 (2017).
102. Kantonen, T. et al. Interindividual variability and lateralization of μ-opioid receptors in the human brain. *NeuroImage* **217**, 116922 (2020).
103. Naganawa, M. et al. First-in-human assessment of 11c-lsn3172176, an m1 muscarinic acetylcholine receptor pet radiotracer. *J. Nucl. Med.* **62**, 553–560 (2021).
104. Nørgaard, M. et al. A high-resolution in vivo atlas of the human brain's benzodiazepine binding site of GABAA receptors. *NeuroImage* **232**, 117878 (2021).
105. Normandin, M. D. et al. Imaging the cannabinoid cb1 receptor in humans with [11c] omar: assessment of kinetic analysis methods, test–retest reproducibility, and gender differences. *J. Cereb. Blood Flow Metab.* **35**, 1313–1322 (2015).
106. Parker, C. A. et al. Human kinetic modeling of the 5HT6 PET radioligand 11C-GSK215083 and its utility for determining occupancy at both 5HT6 and 5HT2A receptors by SB742457 as a potential therapeutic mechanism of action in Alzheimer disease. *J. Nucl. Med.* **56**, 1901–1909 (2015).
107. Sandiego, C. M. et al. Reference region modeling approaches for amphetamine challenge studies with [11C] FLB 457 and PET. *J. Cereb. Blood Flow. Metab.* **35**, 623–629 (2015).
108. Savli, M. et al. Normative database of the serotonergic system in healthy subjects using multi-tracer PET. *NeuroImage* **63**, 447–459 (2012).
109. Smart, K. et al. Sex differences in [11 c] abp688 binding: a positron emission tomography study of mglu5 receptors. *Eur. J. Nucl. Med. Mol. Imaging* **46**, 1179–1183 (2019).
110. Hansen, J. Y. et al. Mapping neurotransmitter systems to the structural and functional organization of the human neocortex. *Nat. Neurosci.* **25**, 1569–1581 (2022).
111. Chen, Q. et al. Longitudinal alterations of frontoparietal and frontotemporal networks predict future creative cognitive ability. *Cereb. Cortex* **28**, 103–115 (2018).
112. Liu, W. et al. Longitudinal test-retest neuroimaging data from healthy young adults in southwest China. *Sci. Data* **4**, 1–9 (2017).
113. Yan, C.-G., Wang, X.-D., Zuo, X.-N. & Zang, Y.-F. DPABI: data processing & analysis for (resting-state) brain imaging. *Neuroinformatics* **14**, 339–351 (2016).
114. Guilford, J. P. *The Nature of Human Intelligence* (1967).
115. Silvia, P. J. et al. Assessing creativity with divergent thinking tasks: exploring the reliability and validity of new subjective scoring methods. *Psychol. Aesthet. Creat. Arts* **2**, 68 (2008).
116. Guo, J., Ge, Y. & Pang, W. The underlying cognitive mechanisms of the rater effect in creativity assessment: The mediating role of perceived semantic distance. *Think. Skills Creat.* **33**, 100572 (2019).
117. Wei, D. et al. Increased resting functional connectivity of the medial prefrontal cortex in creativity by means of cognitive stimulation. *Cortex* **51**, 92–102 (2014).
118. de Souza, L. C. et al. Poor creativity in frontotemporal dementia: a window into the neural bases of the creative mind. *Neuropsychologia* **48**, 3733–3742 (2010).

Acknowledgements

This research was supported by the Major Research Plan of National Social Science Foundation of China (21&ZD312), National Natural Science Foundation of China (32071070), Natural Science Foundation of Chongqing (cstc2019jcyj-msxmX0520, cstc2020jcyj-msxmX0299), the Research Program Funds of the Collaborative Innovation Center of Assessment toward Basic Education Quality at Beijing Normal University, the planned project of Chongqing humanities and Social Sciences (2018PY80, 2019PY51), 111 program (B21036), Fundamental Research Funds for the Central Universities (SWU119007), Chang Jiang Scholars Program, National Outstanding Young People Plan and Chongqing Talent Program, Innovation Research 2035 Pilot Plan of Southwest University (SWUPilotPlan005).

Author contributions

C. Liu, Q.L. Chen and J. Qiu designed the study. C. Liu analyzed the data. C. Liu drafted the manuscript. C. Liu, K.X. Zhuang, D.C. Zeitlen, X.Y. W, Q.Y. Feng, R.E. Beaty contributed to revisions and approved the final version of the manuscript for submission.

Competing interests

The authors declare no competing interests.

Additional information

Supplementary information The online version contains supplementary material available at https://doi.org/10.1038/s42003-024-07007-6.

Correspondence and requests for materials should be addressed to Jiang Qiu.

Peer review information Communications Biology thanks Bernhard Hommel and the other, anonymous, reviewers for their contribution to the peer review of this work. Primary Handling Editor: Benjamin Bessieres.